Puncturing a drop using surfactants

By S. T. THORODDSEN[1], K. TAKEHARA[2], T. G. ETOH[2] AND Y. HATSUKI[2]

[1]Mechanical Engineering, National University of Singapore,
9 Engineering Drive 1, Singapore 117576

[2]Civil and Environmental Engineering, Kinki University, Higashi-Osaka 577-8502, Japan

We present experiments, using an ultra-high-speed video camera, which indicate flow-induced buckling of a surfactant layer on the free surface of a deforming water drop. This results in the 'puncturing' of the liquid surface, sending out a narrow jet. The phenomenon is produced when a water drop falls onto and passes through a hemispherical soap film. The soap film wraps around the drop forming a closed pocket, with a thin layer of air separating the two. This occurs without initial contact between the soap film and the drop liquid, which becomes clear during the subsequent dynamics, as the original film unwraps fully from the drop surface. Under particular conditions the soap film makes contact with the top of the drop, producing a toroidal bubble, which is driven down the drop to form a hemisphere at its bottom. We propose that the resulting rapid reduction in surface area of the bubble leads to overpacking of the surfactant molecules and buckling of the surface, which allows the jet to emerge, from the bottom tip of the drop. Marangoni-driven boundary layers, converging at the bottom, may also play a role in forcing out the jet.

1. Introduction

Surface tension pulls small drops into spherical shape to minimize surface energy. Similar to a balloon, the pressure inside the drop is increased by this tension. Were one able to puncture the surface, i.e. make a localized hole where the surface tension disappears, the liquid would issue out of the hole driven by this overpressure, just like the air out of a punctured tyre.

In general a surfactant such as soap will reduce the strength of the surface tension of a water/air interface by about one half. Therefore the contact of a water drop with a soap solution will locally reduce the surface tension producing changes in the drop shape and generating Marangoni waves. But this is not sufficient to 'puncture' the surface, as would occur if the surface tension were to vanish locally. We have however discovered just such an occurrence, which arises through a set of coincidences when a water drop impacts onto and penetrates through a soap film.

Using a novel ultra-high-speed video camera, Etoh *et al.* (2002, 2003), capable of up to 1 million frames/s we were able to investigate a number of different configurations when a water drop impacts onto a hemispherical soap film, as shown in figure 1, thus identifying the following scenario. The film deforms to form a pocket round the impacting drop. This pocket pinches off at the top, fully enclosing the drop. A thin layer of air separates the film from the drop along its lower side and a pocket of air is trapped on the top. The satellite bubble which is left behind during the pinch-off above the drop, now happens to drift down and hit the top of the film, forcing it to
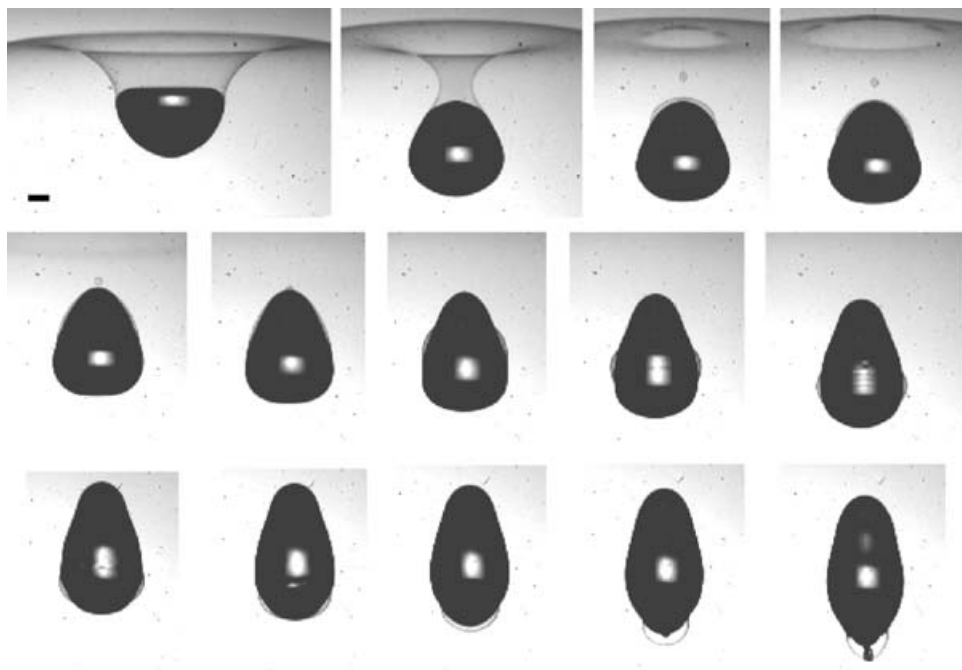
FIGURE 1. The sequence of events following the impact of a water drop onto a hemispherical soap film, showing the propagation of the toroidal bubble and the ejection of a jet at the bottom of the drop. The time difference between the first and second frames is 3.5 ms and 0.5 ms between all the subsequent frames. The scale bar is 1 mm long.

touch the drop liquid. Once contact is made, the film unwraps as shown schematically in figure 5(a). Marangoni forces pull the inner layer of soap molecules down along the drop surface while the air pocket splits to form a torus which propagates down the drop. This propagation is driven by the net surface tension of the soap, which forces open the air gap until it reaches the bottom forming a bottom hemisphere. At this time the bottom tip of the drop ejects a jet of liquid. In the following sections we will describe the details of this phenomenon.

The dynamics and control of surfactant films is an active area of research with a number of applications. They hold great promise in areas from inkjet printing of microdevices to the control of drug delivery. We do not attempt to review the vast literature on these phenomena, but point out the recent overview of capillary and surfactant phenomena given in DeGennes, Brochard-Wyart & Quéré (2004).

2. Experimental setup

The experimental setup is sketched in figure 2. We use a plastic film canister to support the hemispherical soap film. By dipping the open circular top into a soap solution a flat film readily forms across it. The bubble is then blown up by hydrostatic pressure, in the following manner. We puncture a hole in the bottom of the canister. The canister is then stood in a shallow pool of the soap solution, which flows into the bottom, forcing the air up to form the hemispheric cap. The canister used was made of clear plastic from Fuji film with an outer diameter of 31 mm. The radius of curvature of the bubble cap was therefore about 15 mm and the bubble is minimally deformed by gravity. By adding liquid to the pool we can adjust the height of the
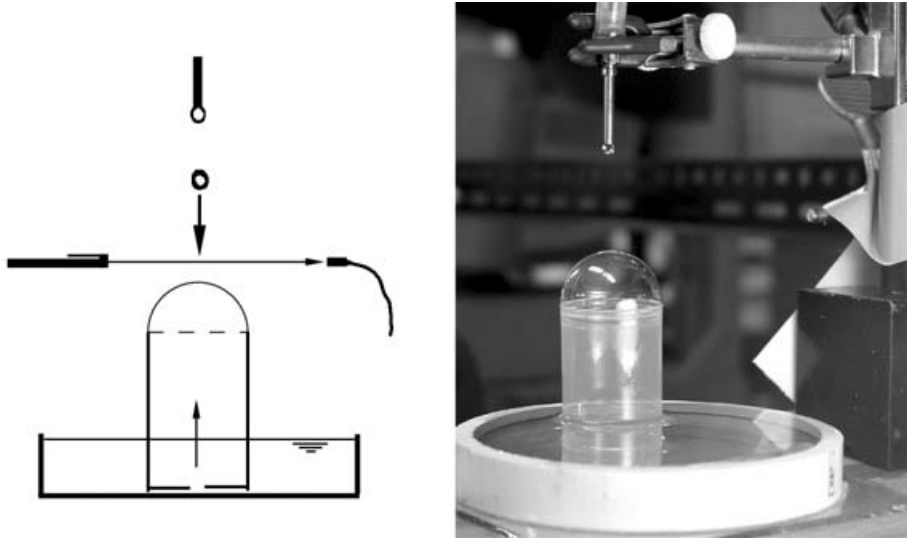
FIGURE 2. Experimental setup.

bubble. Original experiments with a flat soap film were abandoned due to the drainage towards the centre of the film.

The soapy liquid used consisted of 70% deionized water, 25% glycerin and 5% dishwashing soap. The soap solution contains sodium α-olefin sulphonate (20%), fatty acid alkanol amide, sodium alkyl ether sulphate and a trace amount of bacterial stabilizer. The solution is therefore far above the critical micelle concentration (CMC). The surface tension of the solution was $36.6\,\mathrm{dyn\,cm^{-1}}$, measured with a ring tensiometer. The kinematic viscosity was not measured, but is roughly estimated to be about the same as a 30% glycerin solution, i.e. $\nu \simeq 2.3 \times 10^{-6}\,\mathrm{m^2\,s^{-1}}$.

Backlighting was used for the imaging. A high-intensity lamp shone onto one or more sheets of tracing paper to form a silhouette of the phenomenon. We used either a 200 mm macro lens or a long-distance microscope (Questar QM100) to observe the finer details of the process.

Experiments were conducted for a range of impact conditions. The stainless steel needle used in the experiments had an OD of 3.0 mm. The water drop which was generated by the pinch-off from this needle had a diameter of 4.4 mm. The impact velocity was varied by simply changing the release height, mostly at $H \simeq 15\,\mathrm{mm}$ above the film. For the results shown here the Reynolds and Weber numbers based on the drop diameter, fall velocity and surface tension and viscosity of water are, unless otherwise stated, about

$$We_d = \frac{\rho D U^2}{\sigma} = 16, \qquad Re_d = \frac{DU}{\nu} = 2400.$$

2.1. *Ultra-high-speed video camera*

The drop passes through the soap film in a few milliseconds, depending on the drop velocity. However, some of the phenomena observed, such as the closing of the soap cylinder above the drop, occur during a few microseconds. Detailed observations therefore require ultra-high-speed imaging. To capture the dynamics, we use a newly developed ultra-high-speed video camera (Etoh *et al.* 2002, 2003), capable of up to 1 million frames/s. The prototype (Shimadzu Corp.) can acquire 103 consecutive
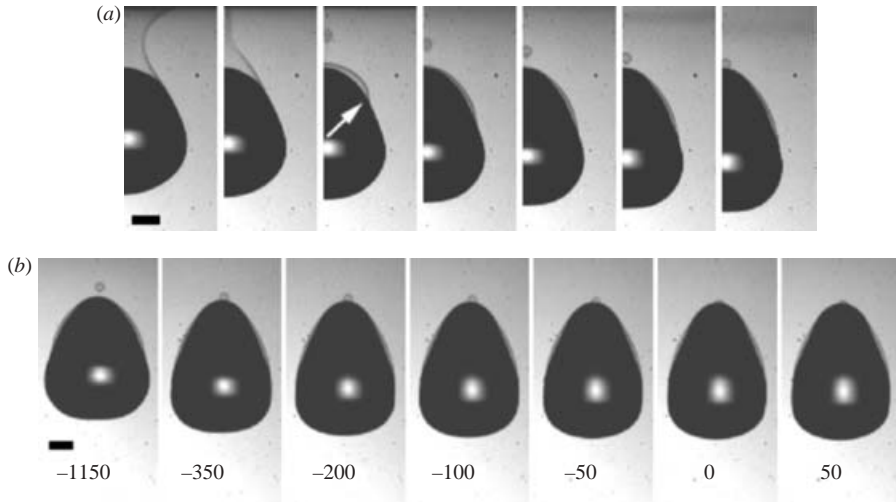
FIGURE 3. The motion of the air pocket and satellite bubble before the soap film contacts with the top of the drop. (*a*) The time between frames is 200 µs. The left side of the panels coincides with the centre of the drop, with the pinched-off satellite bubble lying slightly to the right of centre. (*b*) The approach and contact of the satellite bubble to the top of the drop/soap film. Note how the bubble is suddenly pulled down towards the drop, to mark $t = 0$. Times are in µs. Scale bars are 1 mm long.

frames, with each frame having 260×312 pixel elements irrespective of the frame rate used. The camera records frames continually into the ISIS memory, residing within every pixel, which clears through a drain, until a trigger signal stops the imaging. This allows observations of events occurring before the trigger signal. We have previously used this camera to study the entrapment of air bubbles under a drop impacting onto a flat liquid surface, Thoroddsen, Etoh & Takehara (2003), where additional details are described.

3. Results

Figures 1 and 3 show typical sequences of events which occur as a pure water drop penetrates the film. The film deforms into a pocket around the drop, which pinches off above it. This leaves a 'satellite' soap cylinder, very similar to the liquid cylinder left behind during the pinch-off of a drop from a nozzle. This cylinder contracts to form a small bubble. The dynamics of such a contraction and pinch-off has been studied in detail by Robinson & Steen (2001), for a large soap cylinder supported by two rings. This overall sequence is repeated for all impact velocities.

The thickness of the air film separating the drop from the soap film cannot be measured here. However, for similar impact Weber and Reynolds numbers, the air disk entrapped under a drop impacting onto a liquid pool, without surfactants, was measured to be about 2 µm thick by Thoroddsen *et al.* (2003). The flexibility and stretching of the soap film makes this only a rough order-of-magnitude guess for the air thickness, serving more as an upper bound. We also do not expect this thickness to be uniform around the drop.

3.1. *Motion of the toroidal bubble*

The video clips were analysed to obtain the speed of propagation of the toroidal bubble down the drop. Figure 4 shows the results. For reference the outline of the
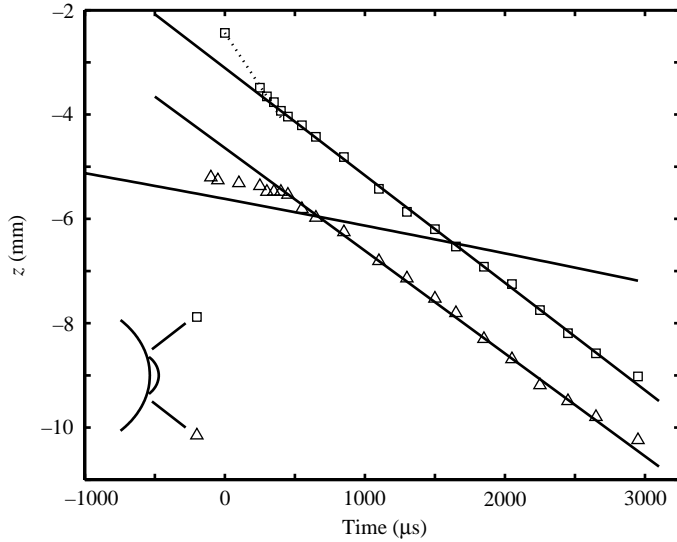
FIGURE 4. The vertical motion of the toroidal bubble down the drop surface. The thick solid line tracks the centre of mass of the drop. The square tracks the top of the toroidal bubble and the triangle the bottom, as indicated in the inset. The dotted line marks the initial motion following the contact of the micro-bubble at the top of the drop.

drop was evaluated by thresholding and the downward motion of its centre of mass was calculated, based on the axisymmetry. The drop free falls at $0.53\,\mathrm{m\,s^{-1}}$ as shown by the thick line in the figure. Acceleration by gravity is minimal over this short duration of time.

The original contact, for this impact condition, is promoted by the satellite bubble, which bumps into the top of the drop. This is not necessary for contact, but gives an accurate estimate of the initial contact time. Figure 3(b) shows the bubble to settle at the top of the drop, sit there for about $350\,\mu\mathrm{s}$, before it is suddenly pulled down, indicating contact. This is used to identify t_o in figure 4. The initial downward motion of the contacting film cannot be observed, as the air film is too thin, but interpolation, shown by the dotted line in figure 4, indicates downwards speed of $4.06\,\mathrm{m\,s^{-1}}$. For the first $450\,\mu\mathrm{s}$ after contact, the lower edge of the toroidal bubble is simply moving down with the drop, until sufficient pressure has developed inside the bubble to 'peel' the soap film from the drop surface as the bubble travels down the drop. Thereafter, the toroidal bubble moves down the drop at close to constant speed, with the best linear fits, giving 2.06 and $1.97\,\mathrm{m\,s^{-1}}$ for the top and bottom edges. The graph ends when the bottom edge has reached the bottom apex of the drop. Relative to the drop, the downward motions following the first contact at the top of the drop therefore start at $3.5\,\mathrm{m\,s^{-1}}$ and then the toroidal bubble proceeds at a vertical speed of $1.5\,\mathrm{m\,s^{-1}}$. Measured along the drop surface, these values would be slightly higher.

3.2. *Pressure inside the toroidal bubble*

The drop undergoes large surface deformations after breaking through the soap film. The air-filled soap bubble can however reach equilibrium pressure much faster. Just before contact with the drop, the first panel in figure 5(b), the film has essentially reached a surface shape of constant mean curvature, within the experimental accuracy.
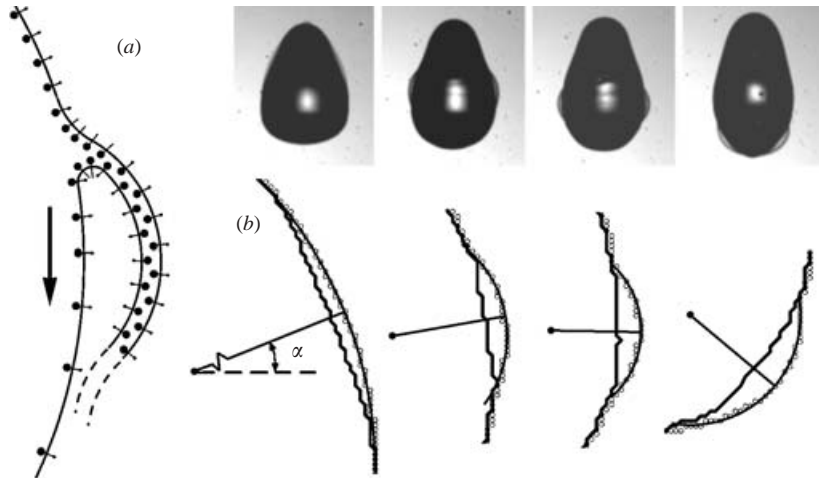
FIGURE 5. The shape of the toroidal bubble. (*a*) Sketch showing the proposed flow of surfactant molecules along the drop surface. (*b*) Traces of the best-fit circles, giving the radius of curvature of the bubbles in the above frames. From left to right the values of the radii (R, R_z) are in mm: (1.66, 4.70); (2.05, 1.27); (2.10, 1.00); (1.36, 1.22), which gives the corresponding internal pressures of $\Delta p = (55, 93, 108, 98)$ Pa.

The internal gauge pressure in the bubble is given by

$$\Delta p = 2\sigma \left(\frac{\cos \alpha}{R} + \frac{1}{R_z} \right)$$

where R is the local radius of the bubble from the axis of symmetry and α is the average tilting angle of the soap film away from the vertical. R_z is the radius of curvature in a vertical plane through the axis of symmetry. Before contact the internal gauge pressure is $\Delta p = 55$ Pa. The same appears true during the downwards motion of the toroidal bubble, which proceeds at nearly a constant, but larger total curvature, giving internal pressure around $\Delta p = 100$ Pa, as shown in figure 5(*b*).

3.3. *The changes in film area*

Frame-by-frame analysis of the video clips was also used to track the surface area of the soap film. First, we verified that the entrapped volume of air is conserved as the toroidal bubble moves down the drop. The top and bottom bubble volumes are the same within the experimental accuracy of about 5%.

The total surface area surrounding the enclosed air, entrapped between the film and the drop, was also integrated from the images. This is used to estimate the surfactant concentration when the jet emerges. Figure 6 shows the change in this surface area, starting from the pinch-off of the film above the drop. The sudden jump in area marks the contact with the drop, which allows the surfactants to spread along the drop surface. The release of surface energy proceeds at approximately a constant rate of $\sigma \, dA/dt = 1.9 \times 10^{-3}$ W using the average surface tension of the water and the soap solution. The area inside the bottom bubble, when the jet emerges, is about 28% of the original inside area of the soap pocket which enclosed the drop at pinch-off.

Figure 7 shows a tiny bubble being pinched off from the top edge of the toroidal bubble. This was occasionally observed as the bubble passes the thickest section of the drop, but our optical arrangement was not set up to detect all such cases.
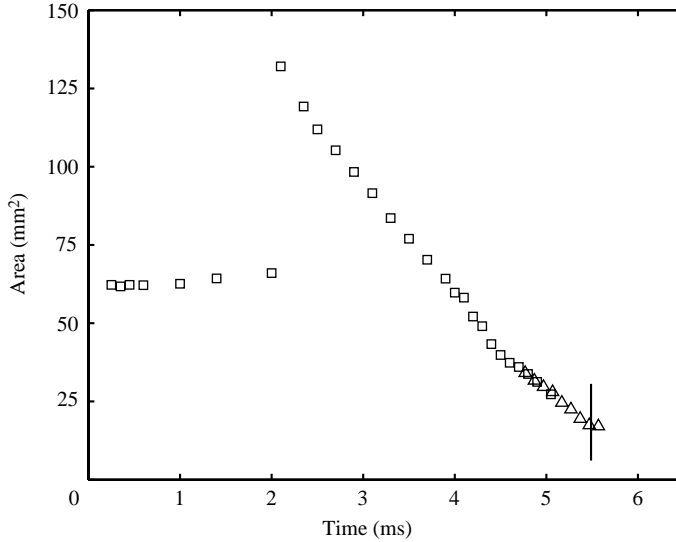
FIGURE 6. The total internal surface area of the enclosed air volume, as the toroidal bubble travels down the drop. The vertical line marks the emergence of the bottom jet. Time zero corresponds here to the pinch-off of the pocket and the jump in area marks the contact of the soap film and the drop, at $t = 0$ in figure 3(*b*). Data are taken from two realizations ($\square$ and $\triangle$), with the time-axis shifted slightly (by ~ 0.1 ms) to match the area of the two.
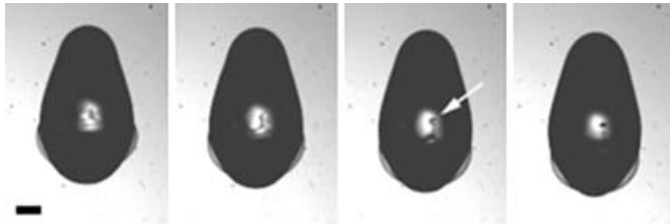
FIGURE 7. Small bubble is pinched off from the top edge of the toroidal bubble. The time between frames is 200 μs. The scale bar is 1 mm long.

3.4. *The bottom jet*

The bottom jet is 230 ± 30 μm across when it emerges. The initial speed relative to the drop is measured at 1.7 ± 0.2 m s^{-1}. This gives Weber and Reynolds numbers for the jet, using jet diameter D_j and velocity U_j, equilibrium σ for the soap solution and viscosity of water, of

$$ We_j = \frac{\rho D_j U_j^2}{\sigma} = 18, \qquad Re_j = \frac{D_j U_j}{\nu} = 412. $$

The jet does not penetrate the bottom soap film, but forms a thicker tip and bends to the side. The jet surface is not smooth, but becomes 'agitated' and irregular, as shown in figure 8. The rest of the drop surface, inside the bottom bubble, becomes irregular about 2 ms after the emergence of the jet, suggesting that buckling is now occurring all along this surface.
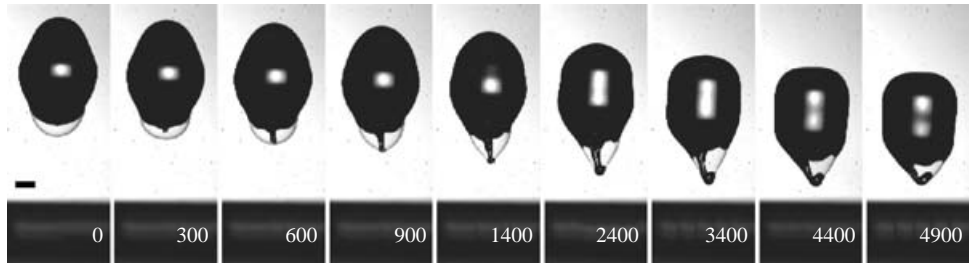
FIGURE 8. The evolution of the bottom jet for $We_d = 12$. Times in µs after the jet first appears. Bar is 1 mm.

4. Discussion and conclusions

4.1. *Motion of toroidal bubble*

The toroidal bubble is driven down the drop to minimize surface energy. The elongated bubble is stretched all the way around the bottom of the drop and should find a minimum surface area as a hemisphere at its bottom. A control volume around the toroidal part of the bubble, figure 5(*a*), shows three free surfaces pulling the bubble downward, whereas only one free surface pulls up. This imbalance in the surface tensions will occur with or without surfactant molecules on the drop surface. During the initial motion, the soap film can simply be contracting, until the soap molecules reach full packing. Thereafter, the pressure inside the toroidal bubble needs to 'peel' the film away from the drop surface.

The surface tension of the pure water, at the fresh surface of the drop, is about twice that of the soap film. This will produce Marangoni stress acting downwards along the drop surface, which will help pry open the air gap, by pulling air into it, like a conveyor belt. This Marangoni stress is however not necessary to force the film from the surface, as is clear from figure 3 (arrow), where the film is separated from the drop surface simply by the film motion following the pinch-off, similar to the 'flapping' of a carpet.

4.2. *The bottom jetting*

We believe the jet emerges owing to overloading of the free surface with the surfactant molecules, making it buckle and lose its ability to support tension, with the same effect as puncturing a hole in the surface. The jetting occurs at the bottom of the drop, along the axis of symmetry, where the Marangoni-driven boundary layers converge to pack the surfactant and produce stagnation pressure to help push out the jet. The Laplace pressure is also largest in this region, of larger drop curvature, but probably plays a secondary role.

The spreading and structure of the surfactant layer, along the drop, will determine the size of the jet, see Jensen (1995) for a review of spreading along a flat surface. The drop liquid here is free of the surfactant and adsorption to the drop surface is therefore not present. Desorption of the surfactant molecules into the drop is probably not significant during this short time, 3.5 ms, from contact to the emergence of the jet. The location of the leading edge of the surfactant can therefore be estimated to spread as $z = K \Delta \sigma^{1/2} t^{3/4} / (\mu \rho)^{1/4}$, as discussed in Dussaud & Troian (1998). Taking the value for the constant $K = 1.5$, the front should spread about 4 mm in the 3.5 ms, which is similar to the actual motion. The bubble is however being pulled rapidly along the surface, which could generate a surfactant front as the surface-tension gradient weakens. The boundary layer thickness is of order $\delta \sim \sqrt{\nu t} \sim 60$ µm, which
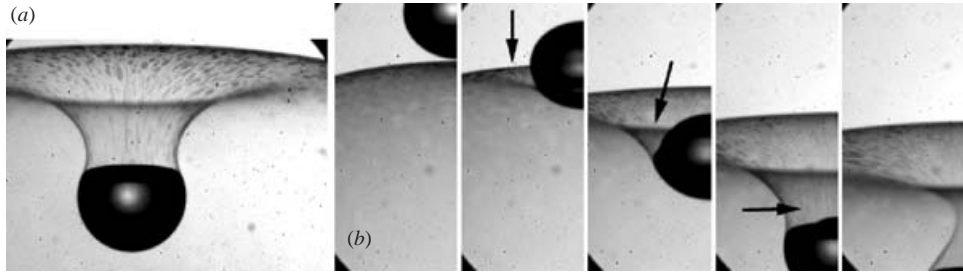
FIGURE 9. The stretching of the soap film. (*a*) Overall view of the stretching of a newly made soap film, just after its formation. (*b*) Tracking of one region in the film. The tracer is barely visible in the images, but can be tracked by following the motion through many frames in the video clip. The dark arches in the corners are simply the edges of the field of view of the lens.

would converge to a stagnation region at the bottom with size of the same order as the emerging jet.

4.3. *Surfactant concentration*

The internal surface area, when the jet emerges, is about 28% of the original pinch-off area of the pocket enclosing the drop. We expect the original hemispherical film to be fully packed with soap molecules, but the penetration of the drop will force significant stretching of the film, thus reducing the initial surface concentration. This is consistent with the significantly smaller surface area at onset of the jet.

The changes in the polar area leading to film buckling is quite complex and varies with the molecular structure of the surfactants but can in principle be determined by Langmuir trough experiments, see discussions in Krueger & Gaver (2000). From their figure 1, one can infer that buckling occurs when the critical surface concentration is of the order of two times the equilibrium value. If the rapidly compressed film behaves accordingly, then the original stretching due to the drop penetration should be about $0.5/0.28 \simeq 1.8$. Figure 9 shows the stretching as a drop penetrates freshly made film, containing patches, which can be tracked. The area of the film, πR_f^2, which ends up in the pocket, $4\pi R_d^2$, was estimated by tracking the patch marked in figure 9(*b*). This patch starts at $R_f/R_d \simeq 1.3$ and ends up slightly below the pinch-off point, which is indeed roughly consistent with the stretching predicted above, i.e. the ratio of the pocket to film areas is $4R_d^2/R_f^2 \simeq 2.3$. Keeping in mind that fresh films will behave differently from films which have drained for some time, these areas suggest that the average surfactant concentration is around two times the equilibrium value, when the jet emerges.

The precise structure of the proposed buckling is beyond the present study. For the buckling or collapse of slowly compressed films there appear to be a few possibilities, as studied by among others Ries & Swift (1987) and Lipp *et al.* (1998). For our purpose it suffices that the surface tension is locally reduced to very low values. To estimate the actual value of σ along the drop inside the bubble, it is instructive to look at the 'contact angle' θ of the film to the drop. Figure 10 shows a closeup of this region after the bubble has almost stopped moving. For a constant value of σ the film would meet the drop at approximately 90°, but here the angle appears significantly smaller, closer to 45°, which would suggest a much weaker tension along the free surface of the drop inside the bubble. Higher resolution images are needed for a more accurate estimate.
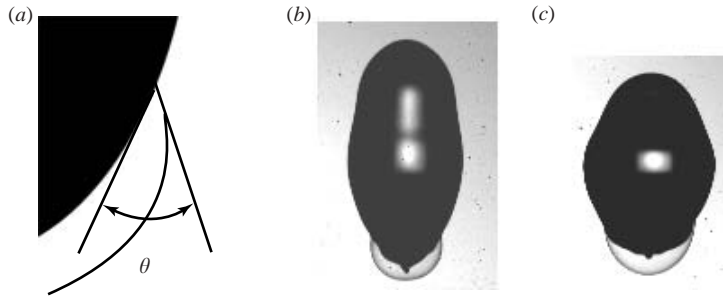
FIGURE 10. The bottom contact angle between the film and the drop, for $We_d = 16$ in (*b*) and for $We_d = 12$ in (*c*).

The proposed 'puncturing' of the surface, is of course quite different from the true holes which can develop in films fully immersed in liquid, as studied by Sandre, Moreaux & Brochard-Wyart (1999) and Brochard-Wyart, DeGennes & Sandre (2000).

In conclusion, we have identified an experimental configuration which produces an intriguing surfactant phenomenon, during the impact of a drop onto a soap film. Rapid reduction in surface area and corresponding overpacking of surfactant molecules, in combination with Marangoni-driven flows, produces jetting from the bottom tip of the drop. More work is needed to understand the kinetics of the surfactant as the Marangoni flow converges at the bottom tip of the drop. Similar configurations where the bottom film does not stop the jet might be used to break drops into smaller droplets. This phenomenon might also prove useful in characterizing surfactants, such as those relevant to the proper functioning of the lungs.

REFERENCES

BROCHARD-WYART, F., DEGENNES, P. G. & SANDRE, O. 2000 Transient pores in stretched vesicles: role of leak-out. *Physica* A **278**, 32–51.

DEGENNES, P. G., BROCHARD-WYART, F. & QUÉRÉ, D. 2004 *Capillarity and Wetting Phenomena, Drops, Bubbles, Pearls, Waves*. Springer.

DUSSAUD, A. D. & TROIAN, S. M. 1998 Dynamics of spontaneous spreading with evaporation on a deep layer. *Phys. Fluids* **10**, 23–38.

ETOH, T. G., POGGEMANN, D., RUCKELSHAUSEN, A. *et al.* 2002 A CCD image sensor of 1 M frames/s for continuous image capturing of 103 frames. *2002 IEEE Intl Solid-State Circuits Conf. Digest of Technical Papers*, vol. 45, pp. 46–47.

ETOH, T. G., POGGEMANN, D., KREIDER, G. *et al.* 2003 An image sensor which captures 100 consecutive frames at 1000000 frames/s. *IEEE Trans. Electron Devices* **50**, No. 1, 144–151.

JENSEN, O. E. 1995 The spreading of insoluable surfactant at the free surface of a deep fluid layer. *J. Fluid Mech.* **293**, 349–378.

KRUEGER, M. A. & GAVER, D. P. 2000 A theoretical model of pulmonary surfactant multilayer collapse under oscillating area conditions. *J. Colloid Interface Sci.* **229**, 353–364.

LIPP, M. M., LEE, K. Y. C., TAKAMOTO, D. Y., ZASADZINKI, J. A. & WARING, A. J. 1998 Coexistence of buckled and flat monolayers. *Phys. Rev. Lett.* **81**, 1650–1653.

RIES, H. E. & SWIFT, H. 1987 Twisted double-layer ribbons and the mechanism for monolayer collapse. *Langmuir* **3**, 853–855.

ROBINSON, N. D. & STEEN, P. H. 2001 Observations of singularity formation during the capillary collapse and bubble pinch-off of a soap film bridge. *J. Colloid Interface Sci.* **241**, 448–458.

SANDRE, O., MOREAUX, L., BROCHARD-WYART, F. 1999 Dynamics of transient pores in stretched vesicles. *Proc. Natl Acad. Sci. USA* **96**, 10591–10596.

THORODDSEN, S. T., ETOH, T. G. & TAKEHARA, K. 2003 Air entrapment under an impacting drop. *J. Fluid Mech.* **478**, 125–134.